

# Conceptual Design and Study of “Engineless” Airplane Using Co-Flow Jet Airfoil

John Aguirre\*, Bao-Yuan Wang<sup>†</sup> and Ge-Cheng Zha<sup>‡</sup>

Dept. of Mechanical and Aerospace Engineering  
University of Miami  
Coral Gables, Florida 33124  
E-mail: j.aguirre1@umiami.edu

## Abstract

In this paper, a new conceptual “Engineless CFJ Aircraft (ECA) is designed and studied by CFD analysis. This aircraft will have no conventional propulsion systems (propeller or jet engine). The new concept airplane will use the fixed wings themselves, in a flying wing configuration, with the inclusion of the newly developed high performance co-flow jet (CFJ) airfoil, to produce both lift and thrust. The energy expenditure for this aircraft will be extremely low. The energy consumption is mainly the power to pump the jet, which can be accomplished by electricity generated by a hydrogen fuel cell. No combustion is therefore needed. The maneuverability and safety of the airplane will be relatively high due to the high stall margin of the CFJ airfoil. CFD aerodynamic analysis is presented for both the two and three dimensional cases for a range of angles of attack.

## 1 Introduction

Conventional aircraft have traditionally made use of propellers or jet engine propulsion systems to generate thrust and the wings, in turn, generate the lift necessary to support the weight of the aircraft. These two systems, the propulsion and lift-generating systems, have always been treated separately. However, with the use of the new Co-Flow Jet airfoil concept, they can be integrated into one, therefore reducing aircraft complexity, and greatly increasing performance and efficiency.

Unlike man-made vehicles, birds, insects and other flying animals do not have separate propulsion and lift systems. They rely on flapping wings to generate both lift and thrust. The down stroke of the flapping wings has a very large angle of attack (AoA) to the relative flow. Vortex shedding at both leading and trailing edges is the dominant flow phenomenon of a bird flapping its wings. The result is that the dynamic circulation of the flapping wing is so high that it generates sufficient lift to support the body weight of a bird, and at the same time, the high circulation generates a

---

\* Graduate Student, AIAA Student Member

<sup>†</sup> Graduate Student

<sup>‡</sup> Associate Professor, AIAA Member

very strong low pressure suction at the wing leading edge that results in a net thrust. Ornithopters use the same principle to fly, however, they are generally limited to very small unmanned air vehicles (UAV). This is generally due to the fact that driving the flapping wings for large aircraft is very difficult and inefficient. From studying bird flight, we can deduce that if the circulation is sufficiently high, a wing can generate both lift and thrust.

For this aircraft, the new concept of the co-flow jet airfoil will be used to produce both lift and thrust. The co-flow jet airfoil was recently developed by Zha et al.[1, 2, 3, 4]. The simple concept of the CFJ airfoil is capable of generating extraordinary performance with a net zero drag (for cruise) or a net negative drag (thrust, for acceleration), as well as extremely high lift and stall margin. The inclusion of a flying wing design takes further advantage of the CFJ airfoil by increasing the area percentage over which it is present in the aircraft. By using such a configuration, the CFJ airfoil will be active even within the fuselage section of the aircraft.

This concept aircraft has the advantage of having a wide range of applications. It can be used for unmanned reconnaissance aircraft, small personal aircraft, commercial airliners, and in many other applications. It has even been proposed that the CFJ can be used to enhance the performance of commercial aircraft already in wide use. The new concept “Engineless airplane is not just useful for flight on Earth, but also for exploratory missions to Mars. The “Engineless CFJ airplane is particularly well suited for flight in the Martian atmosphere due to reduced energy consumption, enhanced maneuverability and safety, extremely short take off/landing distance, soft landing and take off with very low stall velocity, and some other advanced features. These features are desirable due to the limited amount of fuel that can be carried in a mission to Mars, limited take-off and landing space, as well as the challenges of flying in a low density atmosphere in a laminar flow regime[5]. The CFJ airplane will be very promising for flight in both the Earth and Martian atmospheres.

## 2 Co-Flow Jet Airfoil Concept

In the Co-Flow Jet Airfoil concept [1, 2, 3, 4], an injection slot near leading edge and a suction slot near trailing edge on the airfoil suction surface are introduced onto the baseline airfoil as sketched in Fig.6. A high energy jet is injected near the leading edge in the same direction of the main flow and the same amount of mass flow is sucked near trailing edge. The jet is recirculated and is maintained at zero-net mass flux flow control. The fundamental mechanism is that the severe adverse pressure gradient on the suction surface strongly augments the turbulent shear layer mixing between the main flow and the jet[6]. The mixing then creates the lateral transport of energy from the jet to the main flow and allows the main flow to overcome the large adverse pressure gradient and remain attached even at high angles of attack. The stall margin is hence significantly increased. At the same time, the high momentum jet drastically increases the circulation, which significantly augments lift, reduces drag or even generates thrust (net negative drag), much like a bird wing. Fig.2 shows a typical comparison where the baseline airfoil has a massive separation at high angle of attack, whereas the CFJ airfoil has a very well attached flow[2, 1]. To most effectively make use of the adverse pressure gradient to enhance mixing, the injection slot must be located downstream of the leading edge suction peak.

In [1, 2], an overview of different flow control methods is given. Compared with the circulation control (CC) airfoil, the working mechanism of CFJ airfoil is different. A CC airfoil relies on large leading edge (LE) or trailing edge (TE) to have the Coanda effect and enhance circulation.

The large TE or LE may generate large drag during cruise. The CFJ airfoil relies on the wall jet mixing to energize the main flow and overcome the adverse pressure gradient so that the flow can induce high circulation and remain attached at high AoA. The CC airfoil dumps away the jet mass flow, which is a considerable penalty to the propulsion system. The CFJ airfoil, on the other hand, recirculates the jet mass flow and achieves the zero net jet mass flux to have very low energy expenditure. Compared with the synthetic jet flow control, the enhancement of airfoil performance by the CFJ airfoil is much more drastic because the interaction of the main flow with the synthetic jet generated either by acoustic waves or plasma is generally weak. The CFJ airfoil simultaneously achieves three radical improvements at low energy expenditure: lift enhancement, stall margin increase, and drag reduction or thrust generation.

In [4], the control volume analysis indicates that the drag or thrust of a CFJ airfoil measured in the wind tunnel is the actual force acting on the airfoil or aircraft system in the stream-wise direction. This is not the same as the CC airfoil, which must consider the equivalent drag due to the suction penalty from the free-stream. For a CC airfoil, the equivalent drag is significantly larger than the drag measured in a wind tunnel and is also substantially larger than the drag of a CFJ airfoil. For a CFJ airfoil, the suction penalty is already included in the measured drag and is off set by the higher circulation and stronger leading edge suction induced by the CFJ[4, 7]. The drag reduction mechanism of a CFJ airfoil is not based on the conventional concept to reduce the skin friction. Instead, it relies on the help of the pressure resultant force, which overwhelms the skin friction. When the leading edge suction is very strong, the low pressure at leading edge results in a resultant force that is forward-pointing and is greater than the skin friction. Thus a thrust is produced. When a thrust is generated by the wing, conceptually, no conventional engines are needed.

### **3 The Concept of “Engineless Aircraft Using CFJ Airfoil**

The concept of “Engineless Aircraft using the CFJ airfoil would not need to use any propeller or jet engine system because the CFJ airfoil itself is capable of generating thrust, which can be used to overcome the 3-D induced drag due to tip vortices. The flying wing configuration is most suitable for such an airplane because the CFJ airfoil can cover the entire aircraft surface to achieve the maximum benefit. This flying wing will basically be a wing made from the CFJ airfoil, which generates lift and thrust wherever it is applied. Thus, the only drag that needs to be overcome by the CFJ airfoil thrust would be the induced drag due to tip vortices. In order to operate, the airplane needs a pumping system to draw the jet mass flow near the trailing edge and inject the jet near the leading edge as sketched in Fig.6. At different phases of the flight mission, the lift and thrust can be controlled by adjusting the jet strength. At take off, a strong jet will be used to generate high thrust and high lift. At cruise, mild jet will be used due to lower lift coefficient and thrust required. At landing, the jet will be adjusted to let the CFJ airplane fly at high angle of attack with high lift and high drag.

A conventional airplane draws the air flow from the free-stream environment through the engine inlet, energizes the air through the combustion process, and then exhausts the high momentum air to the environment through the engine nozzle. Such a process is purely for thrust generation and has no interaction with the wing. The energy transfer from the chemical energy of combustion to mechanical energy (momentum increase) is usually very inefficient and accompanies a very large thermal energy (total enthalpy) loss of 50% or more.

A CFJ wing draws the air flow on the suction surface of the wing near the trailing edge, pressurizes the air within the wing and then exhausts the same amount of air flow near the wing leading edge. Such a process has a direct interaction with the wing and enhances the wing lift by inducing a large circulation and generates a thrust at the same time. The mass flow of the jet will be substantially less than that of a jet engine. The jet recirculating or pumping process (suction and injection) needs much less power than running a jet engine and can be done by electric power. The energy transfer is from mechanical energy (pumping the CFJ) to mechanical energy (high momentum injection jet) and therefore the efficiency is much higher. No combustion process is needed and hence zero emission will be produced.

### 3.1 Vision and Impacts

#### 3.1.1 Low Energy Expenditure, Long Range and Endurance

The power required to pump the jet for this aircraft will be significantly less than the power required to run a conventional jet engine. When the power is consumed to generate the CFJ and enhance lift, it will also reduce the drag, and at low angles of attack produce thrust. For conventional airplanes, the power system is used only to overcome the drag without enhancing lift coefficient. The equivalent L/D of the CFJ airplane hence will be much higher than that of the conventional airplane. Since the lift coefficient of the CFJ aircraft element is significantly higher than the conventional airfoil, the overall lifting surface area to have the same payload will thus be much smaller. The weight of the airplane and the drag due to the whetted surface will be also significantly reduced. With no aircraft engines, the weight of the engines and the drag due to the engine nacelles and captured area will also be removed. The reduced weight and drag will further reduce the energy consumption.

The power consumption of the pump that drives the CFJ jet can be defined as:

$$P = \frac{\dot{m}c_p T_{01}}{\eta} \left( \left[ \frac{p_{01}}{p_{02}} \right]^{\frac{\gamma-1}{\gamma}} - 1 \right) \quad (1)$$

where  $c_p$  is the specific heta capacity at constant pressure, taken to be  $1003.4J/kg \cdot K$ ,  $\gamma$  is the ration of specific heats 1.4, and  $\eta$  is the efficiency of the pump. Assuming a small unmanned recinaissance-type aircraft with a chord length of  $1.16m$ , the power necessary to drive this pump at a take-off speed of  $M = 0.1$  is only  $79.1W$ .

As seen from Eq. (1), the power required to pump the jet is determined by the ratio of the total pressure at the injection and suction and the mass flow rate of the jet. The jet pressure ratio for the ECA has been calculated to be about 1.1, whereas the ratios seen with conventional jet engines can be as high as 40. Compared with a jet engine system, the reduction of power required comes from the following 5 sources:

1. The mass flow rate of the jet is much smaller than the mass flow rate of the jet engine; conservative estimations show that the maximum jet mass flow rate would not exceed 30% of that of a conventional jet engine.
2. The total pressure ratio to pump the jet will be much smaller than the total pressure ratio of a jet engine compressor. For example, if the injection total pressure is 2 times the static

pressure in the injection slot area, the injection jet Mach number will be 1.05. Usually, the injection jet speed will be limited to lower than sonic speed for subsonic flight. CFD analysis show that the velocity at the jet injection do not exceed a Mach number of 0.65.

3. The CFJ injection and suction are at the most energy efficient locations. The suction is at near trailing edge where the pressure is the highest on the airfoil except the LE stagnation point. Injection is right downstream of the leading edge suction peak where the pressure is the lowest. The pressure gradient is favorable to recirculate the jet and minimize the power required to pump and energize the jet.
4. No combustion is needed and hence very little thermal loss occurs.
5. The overall “Engineless airplane weight and drag is much less than the conventional airplane. The energy expenditure is hence greatly reduced.

Conceptually, the estimation shows that the reduction of the power required for an “Engineless CFJ airplane could be very significantly. The lower power consumption of a CFJ airplane will give much longer range and endurance than a conventional airplane.

### **3.1.2 Extremely Short Take Off/Landing Distance**

The take off/landing distances and the stall velocity are determined only by the maximum lift coefficient. The CFJ airplane will hence have extremely short take off/landing (ESTOL) distance due to the very high maximum lift coefficient. For the same reason, the stall velocity will be significantly lower than the conventional airplane. The lower stall velocity will allow soft landing and take off at substantially lower speed. Another important use of CFJ airfoil during take off/landing is to enhance the subsonic performance of a supersonic wing for a supersonic airplane.

### **3.1.3 High Maneuverability and Safety**

Due to the high stall margin, the CFJ airplane will have significantly higher maneuverability and safety margin to resist severe weather conditions, such as unexpected gusts of wind. The high stall margin is also particular useful for Mars airplanes to resist flow separation and stall at low Reynolds number.

### **3.1.4 Low Noise with No High Lift System**

Since the CFJ airplane can generate very high lift, the conventional high lift flap and slat system, which is the primary noise source at landing, is not needed. Without the high lift system, the noise at landing will be reduced significantly. Since the CFJ occurs on the upper surface of the airplane, even though the CFJ mixing itself may generate a certain noise, the noise will mostly scatter and radiate upper ward and will not have a large effect on the residents on the ground.

## **3.2 Jet effects on CFJ aircraft performance**

By using a control volume analysis, Zha et al. derived an expression for the force effect of the injection and suction jets on the CFJ wing [4]. In keeping with Newton’s third law, at the injection

and suction slots, the high velocity flow produces a reactive force which must be taken into account in the drag and lift calculations. The expressions for these reaction forces are given as:

$$F_{x_{cfj}} = \dot{m}_j V_{j1} + (p_{0j1} A_{j1}) * \cos(\theta_1 - \alpha) - \gamma(\dot{m}_j V_{j2} + (p_{j2} A_{j2}) * \cos(\theta_2 + \alpha)) \quad (2)$$

$$F_{y_{cfj}} = \dot{m}_j V_{j1} + (p_{0j1} A_{j1}) * \sin(\theta_1 - \alpha) - \gamma(\dot{m}_j V_{j2} + (p_{j2} A_{j2}) * \sin(\theta_2 + \alpha)) \quad (3)$$

Where the subscripts 1 and 2 refer to the injection and suction respectively,  $\dot{m}_j$  is the jet mass-flow rate,  $V_j$  is the jet velocity,  $p_{0j}$  is the jet total pressure,  $A_j$  is the slot area,  $\alpha$  is the wing angle of attack, and  $\theta_1$  and  $\theta_2$  are the angles that the injection and suction slots, respectively, make to the vertical.

The total modified lift and drag on the wing can then be expressed as:

$$D = R'_x - F_{x_{cfj}} \quad (4)$$

$$L = R'_y - F_{y_{cfj}} \quad (5)$$

These quantities modify the forces calculated from the surface integral,  $R'_x$  and  $R'_y$ , in order to correct for the reaction forces induced by the jet effect. It is expected, as can be seen from equations 2 and 3, that the corrected Lift will decrease when  $v_{j1} > 0$  and increase when  $v_{j1} < 0$ .

## 4 Flying Wing CFJ Airframe Design

Unlike most conventional aircraft, where the wings and fuselage are separate structures, the “Engineless CFJ Aircraft will make use of an airframe where both of these components are incorporated into a single, blended body as shown in Figure 5. This is called a Flying Wing configuration, because the entire aircraft acts as an effective wing. Because the fuselage has the same airfoil cross section as the wings, it acts as an extension of the same and thus produces additional lift. This feature also allows for an increased coverage area for the CFJ device, therefore increasing the benefits gained from using it. The planform of the aircraft was chosen such that the desired aspect ratio of about  $AR = 4$  was achieved, while allowing the fuselage section to be thicker than the wings for storage and payload purposes, and still having the same airfoil cross-section. The wings are not highly swept, because the target mission for this study would not near sonic speeds. For takeoff, a Mach number of 0.1 would be sufficient, and a Mach number of 0.3 for cruise. Future studies will be conducted at higher Mach numbers.

A flying wing design also allows for a reduction in the wingspan of the aircraft. Because the fuselage surface is no longer “wasted”, but made to produce lift, the aircraft can produce more lift with a shorter wingspan. This feature is desirable particularly for Martian applications because, in order to reach Mars, the aircraft must be packaged within an aeroshell. The goal is generally to be able to fit the aircraft within an aeroshell while minimizing the number of folds necessary. An aircraft which needs to unfold once it is deployed into the atmosphere is generally less stable and safe due to the increased complexity. An increased number of folds will also increase the probability of failure during deployment, which is the most critical step during the aircraft’s mission [5].

The baseline airfoil chosen for this study is the NACA 6425 airfoil, which can be seen in Figure 6. This airfoil has a camber of 6% located 40% from the leading edge, with a maximum thickness of 25% of the chord. This airfoil was chosen for its moderate camber and high thickness. The high thickness would allow for comfortable placement of all of the CFJ components, such as the pump and ducting. Also, airfoils with high thicknesses will produce higher lift as long as the air flow remains attached. Conventional aircraft shy away from thicknesses higher than 15% due to the increased risk of flow separation. However, with the use of the CFJ device, a higher thickness airfoil can be used without fear of separation occurring, and therefore an even higher lift can be achieved. A moderate camber was chosen in order to reduce the effect of wing-tip vortices. A higher camber airfoil will produce a higher lift, but there is a penalty in the form of stronger induced drag from wing-tip vortices. The NACA 6425 was found to have a good balance in lift produced versus induced drag.

The CFJ airfoil is then created from the baseline airfoil NACA 6425 with the injection slot opened at 7% from leading and suction slot opened at 80% from leading edge. The injection slot size is 0.65% of the chord and the suction slot is 1.96% of the chord. The CFJ airfoil configuration is also shown in Fig. 6, which is the airfoil to construct the flying wing CFJ airplane shown in Fig. 5.

The following table gives some specifications of the CFJ airplane design in this paper:

Wing Span	2.4 m
Root Chord Length	1.16 m
AR	4.0
CFJ Area	1.24 $m^2$
Airfoil thicness	25%
Cruise Mach	0.3
Cruise Altitude	20,000 ft
Weight	104.8 kg
Payload	100 kg
Take-Off Thrust	99.8 kg
Take-Off Lift	542.8 kg
Take-Off Velocity	64 m/s
Take-Off Distance	239.5 m

Table 1: Aircraft specification

## 5 CFD Analysis and Results

A Computational Fluid Dynamics (CFD) study has is being performed for this concept “Engineless CFJ Airplane, which shows its increased performance over a conventional aircraft. CFD analysis was performed for both the two-dimensional and three-dimensional cases at a range of angles of attack (AoA) using both the baseline and CFJ airfoil. The simulations were run at a Reynolds number of  $2 \times 10^6$  and a Mach number of 0.1.

The CFD solver is an in house code solving the 3D Reynolds Averaged Navier-Stokes equations (RANS) [8, 9, 10]. The Roe scheme and a low diffusion E-CUSP schemes are used for the inviscid

fluxes with 3rd order MUSCL type differencing. A 2nd order central differencing is used for the viscous terms. The Baldwin-Lomax turbulence model is used for its high efficiency. Implicit Gauss-Seidel line relaxation is used for the time marching. This code has been intensively validated for various 2D and 3D steady and unsteady flows.

## 5.1 Two-Dimensional Analysis

For the 2-D case, the simulations show that separation occurs for the baseline airfoil at  $16^\circ$  AoA, while flow separation (stall) occurs at  $35^\circ$  AoA for the CFJ airfoil, a  $19^\circ$  difference, as shown in Table 2 and Fig. 9. This constitutes a significant increase in performance because a higher lift can be produced without the danger of stalling, even at a relatively low Mach number of 0.1. These results imply that the stall velocity for such an aircraft would be drastically reduced, and operational angle of attack vastly increased. A lower stall velocity and increased lift can lead to reduced take-off and landing distances, which is a very highly desirable trait.

Furthermore, it can be seen that the two-dimensional drag coefficient  $C_d$  is negative in the case of the CFJ airfoil at angles of attack as high as  $20^\circ$ . The drag coefficient becomes positive at high angles of attack because the form drag has become large enough at that point to overcome the thrust generated by the CFJ airfoil. However, it would be improbable that the aircraft would ever need to fly in conditions where the angle of attack were so high. Even at high angles of attack, however, the drag coefficient of the CFJ airfoil is much lower than that of the baseline airfoil, reducing the high drag generated at such conditions.

AoA	BL $C_l$	CFJ $C_l$	BL $C_d$	CFJ $C_d$
0	0.0542	2.8517	0.0232	-0.9855
10	1.3946	3.9734	0.0408	-0.5939
15	1.5225	5.0729	0.0558	-0.3168
20	1.4431	5.4402	0.0686	-0.1217
30	1.1147	6.5638	0.1690	0.2613
35	0.9348	5.5526	0.2342	0.1913

Table 2: 2-D CFD results for aerodynamic parameters of baseline (BL) airfoil and CFJ airfoil.

## 5.2 Three-Dimensional Analysis

3-D CFD simulations have been performed for the three-dimensional “Engineless CFJ aircraft in a range of angles of attack from  $-5^\circ$  to  $45^\circ$ , using the same Reynolds and Mach numbers as in the 2-D case. The results obtained from the post-processing of the data were corrected to include the jet effects as defined in eq. (2) to (5) [4].

Fig. 10 is the 3D lift vs AoA and show that flow separates at a very high angle of attack, about  $35^\circ$ . Fig. 10 is the 3D drag polar indicates that the 3-D drag coefficient remains negative within a range of angles of attack of about  $-5^\circ$  to  $10^\circ$ . After this point, the form drag is large enough to offset the thrust produced by the CFJ device.

As can be seen from figure 13, the low pressure of the leading suction effect (blue) contributes significantly to generate the thrust. The momentum coefficient  $C_\mu$  remains relatively constant at the value of about 0.29 throughout a range of angles of attack, as can be seen from Fig. 12.

Wake profile plots for the aircraft at different sections along the wing show that the drag is more highly negative at the root of the aircraft, and becomes positive towards the wingtips, where induced drag becomes significant. This can be seen from Fig. 14. However, when averaged over the wingspan, the net drag is negative at low angles of attack. Normally, the wake of a wing features flow that is slower than in surrounding areas. However, the CFJ wake is particular in that the flow there is dramatically faster than in surrounding areas, as can see from Figure 8. As mentioned before, this type of wake profile will lead to a net thrust being produced [1, 4, 11]. The increase in velocity in the wake can also be seen in Fig. 15, which also shows 3D streamlines above and below the wing.

A breakdown of the different sources of drag for this aircraft can be seen in Fig. 16. From this figure, it is clear that the majority of the positive drag contribution for the ECA comes from the induced drag caused by wing-tip vortices, this is the  $y$ -component of the pressure drag. In both the  $x$  and  $y$  directions, the pressure drag greatly overwhelms the friction drag. It is hence expected that the higher aspect ratio will further increase the thrust and AoA range that generates thrust.

Fig. 17 shows the 3D streamlines that illustrate the extent of these vortices. The figure shows streamlines up to 20 chord lengths aft of the wing.

By plotting the pressure coefficient  $C_p$  along the chord for different locations along the wingspan, we can gain some further insight into the forces acting on the aircraft. Figure 18 shows the pressure coefficient at the root of the flying wing, whereas Figure 19 shows the pressure coefficient at the midspan of the wing.  $C_p$  is plotted in three different sections, the top, bottom, and CFJ sections of the airfoil surface. Discrete jumps can be seen at the points where flow is injected and suctioned into the wing. These discrete jumps are due to the sudden change in flow conditions and geometry at those points. The aircraft was modeled with a circular trailing edge, as opposed to a sharp one, therefore there are also rapid changes in the section on the trailing edge. On the areas of more constant geometry, however the  $C_p$  curve has a more smooth variation. At the root of the airfoil, we can see that the lift, that is, the area between the curves, remains more or less constant thought the length of the airfoil. At midspan, however, the bulk of the lift contribution comes from the front of the wing, where there is a higher difference in pressures. From Fig. 13 we can see that this is due to the much lower pressure encountered on the front of the suction surface within the CFJ slot at a position further along the wingspan (blue area in plot).

## 6 Conclusions

The CFJ “Engineless” Airplane concept, while still requiring further study, is proving to be promising in its significant improvements over baseline performance. The use of the CFJ device in an aircraft has been shown to have the effect of significantly increasing lift, reducing drag, providing thrust, and reducing fuel consumption over existing technologies. All of these improvements promise to reduce the resources necessary to operate aircraft, which has become a concern of very high priority for aircraft operators. The CEA concept can be expanded to include military, commercial, and even personal applications.

Within the next months, the studies described in this paper will be expanded to cover further aspect ratios, slot sizes, mach numbers, etc. in order to have a clearer and more profound understanding of the effects and benefits of this promising new technology. It is our goal to be able to perform wind-tunnel testing to verify the CFD results presented here.

## 7 Acknowledgment

This research is supported by ARO/AFOSR Grant 50827-RT-ISP, monitored by Rhett Jefferies (AFOSR) and Jenny Haire (ARO).

## References

- [1] G.-C. Zha and D. C. Paxton, "A Novel Flow Control Method for Airfoil Performance Enhancement Using Co-Flow Jet." Chapter 10, *Applications of Circulation Control Technologies*, p. 293-314, Vol. 214, Progress in Astronautics and Aeronautics, AIAA Book Series, Editors: Joslin, R. D. and Jones, G.S., 2006.
- [2] G.-C. Zha, B. Carroll, C. Paxton, A. Conley, and A. Wells, "High Performance Airfoil with Co-Flow Jet Flow Control." AIAA-Paper-2005-1260, Jan. 2005, submitted for publication in AIAA Journal.
- [3] G.-C. Zha, C. Paxton, A. Conley, A. Wells, and B. Carroll, "Effect of Injection Slot Size on High Performance Co-Flow Jet Airfoil," *AIAA Journal of Aircraft*, vol. 43, 2006.
- [4] G.-C. Zha and W. Gao, "Analysis of Jet Effects on Co-Flow Jet Airfoil Performance with Integrated Propulsion System." AIAA Paper 2006-0102, AIAA 44th Aerospace Sciences Meeting and Exhibit, January 8-12, 2006.
- [5] J. Aguirre, V. Casado, N. Chamie, and G.-C. Zha, "Mars Intelligent Reconnaissance Aerial Ground Explorer (MIRAGE)." AIAA Paper 2007-0244, Jan. 8-12, 45th AIAA Aerospace Sciences Meeting and Exhibit,, also NASA Revolutionary Aerospace System Concept-Academic Linkage, Forum 2006, Cape Canaveral, FL, May 21-24, 2006.
- [6] E. M. Greitzer, C. S. Tan, and M. B. Graf, *Internal Flow*. Cambridge University Press, 2004.
- [7] W. Zha, G.-C. and Gao, C. D. Paxton, and A. Palewicz, "Numerical Investigation of Co-Flow Jet Airfoil with and without Suction." AIAA Paper 2006-1061, 2006.
- [8] G.-C. Zha and Z.-J. Hu, "Calculation of Transonic Internal Flows Using an Efficient High Resolution Upwind Scheme," *AIAA Journal*, vol. 42, No. 2, pp. 205-214, 2004.
- [9] Z.-J. Hu and G.-C. Zha, "Simulation of 3D Flows of Propulsion Systems Using an Efficient Low Diffusion E-CUSP Upwind Scheme." AIAA Paper 2004-3928, 40th AIAA/ASME/SAE/ASEE Joint Propulsion Conference and Exhibit, 11 - 14 July 2004.
- [10] X.-Y. Chen, G.-C. Zha, and M.-T. Yang, "Numerical simulation of 3-d wing flutter with fully coupled fluid-structural interaction," pp. 856-867, June 2007.
- [11] G.-C. Zha and W. Gao, "Analysis of Jet Effects on Co-Flow Jet Airfoil Performance with Integrated Propulsion System," January 2006.

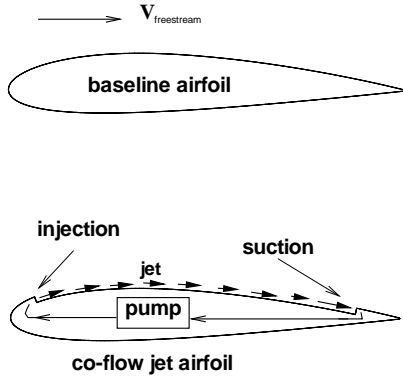


Figure 1: Baseline NACA2415 and CFJ Airfoil

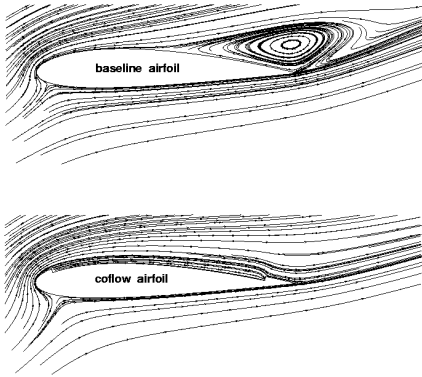


Figure 2: Flow field for the baseline NACA2415 and CFJ Airfoil at high angle of attack

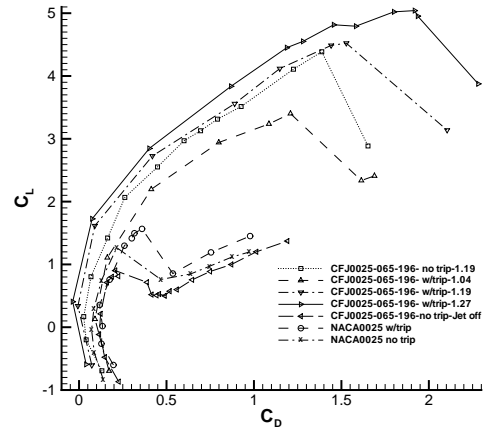


Figure 3: Measured drag polar of CFJ0025-065-196 airfoil.

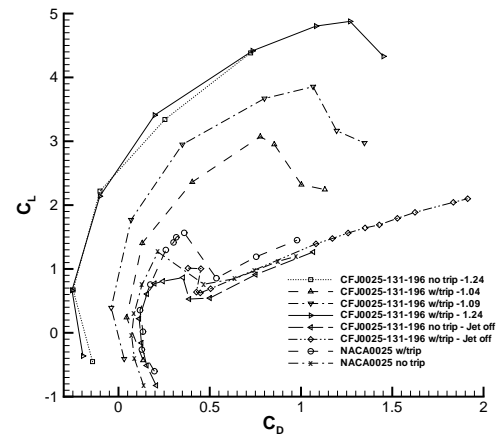


Figure 4: Measured drag polar of CFJ0025-131-196 airfoil.

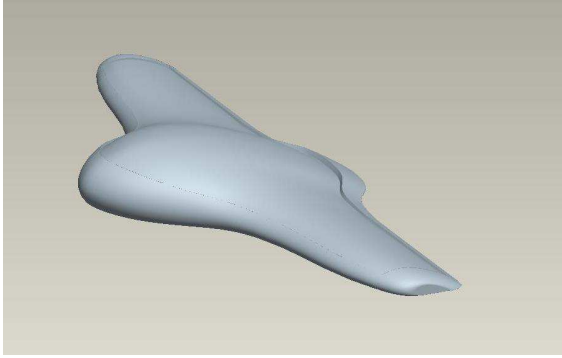


Figure 5: "Engineless Aircraft concept using Flying Wing and CFJ Airfoil"

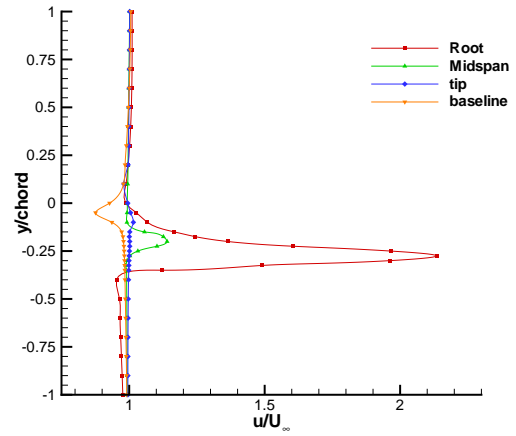


Figure 8: 3-D Wake profile plot for  $AoA = 0^\circ$

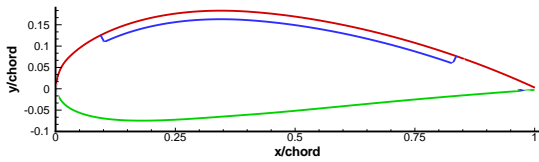


Figure 6: Baseline NACA 6425 airfoil configuration

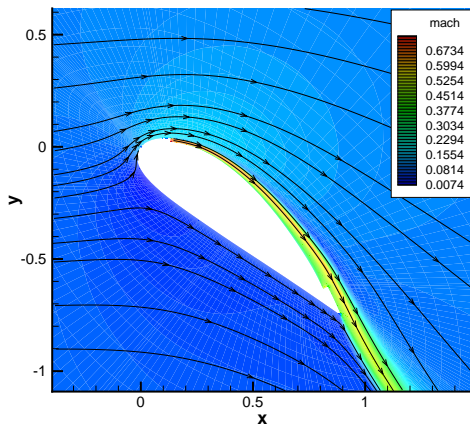


Figure 7: 3-D Streamlines at root for  $AoA = 40^\circ$  showing attached flow

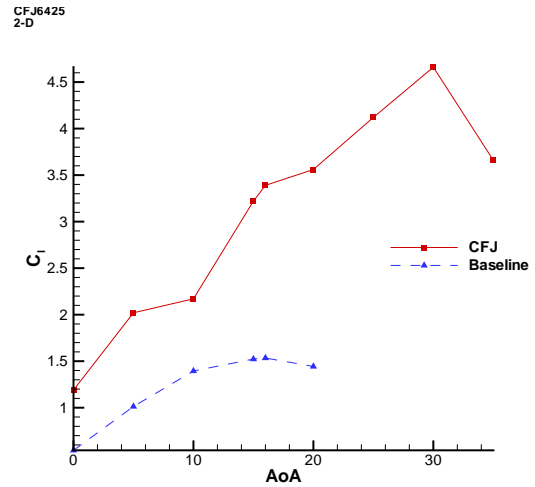


Figure 9: 2-D CFJ Coefficient of Lift versus  $\alpha$  compared with baseline

6425  
AR = 4

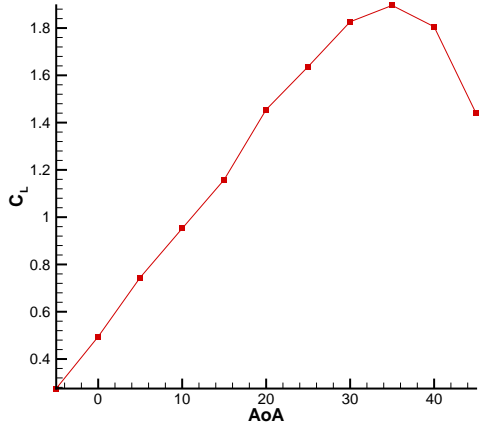


Figure 10: 3-D Coefficient of lift versus angle of attack

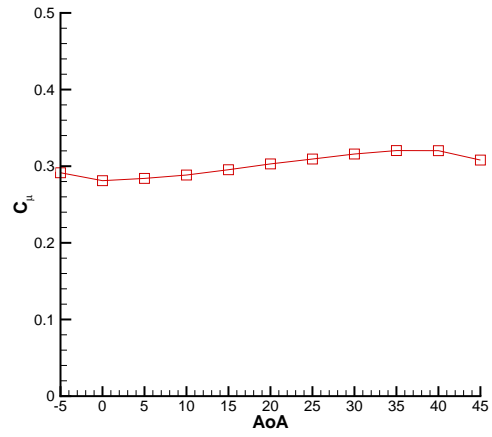


Figure 12: Momentum Coefficient  $C_{\mu}$  versus angle of attack

6425  
AR = 4

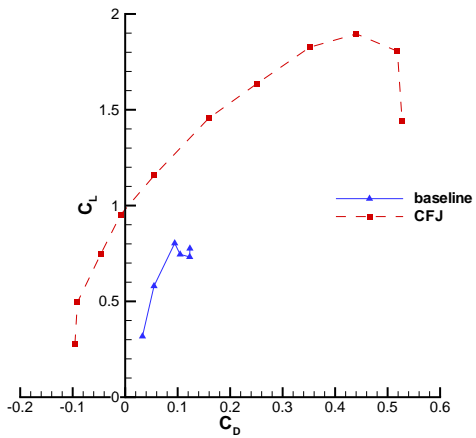


Figure 11: CFJ 3-D Drag polar compared to baseline

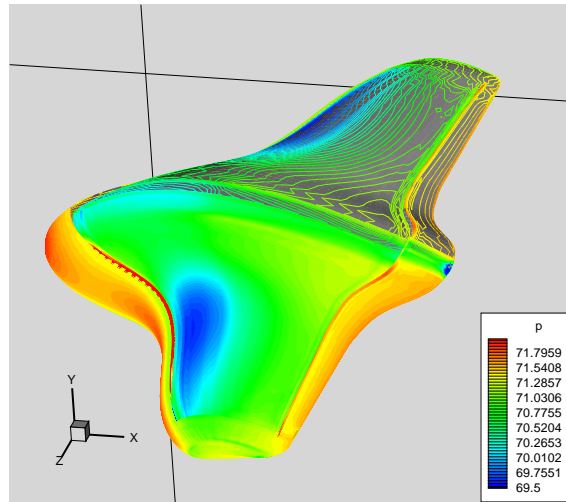


Figure 13: 3-D Surface pressure contours at  $AoA = 0^\circ$

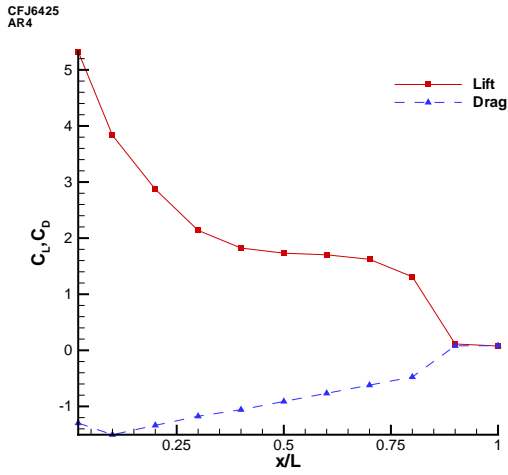


Figure 14: Lift and Drag profile at  $AoA = 0^\circ$  along wing span

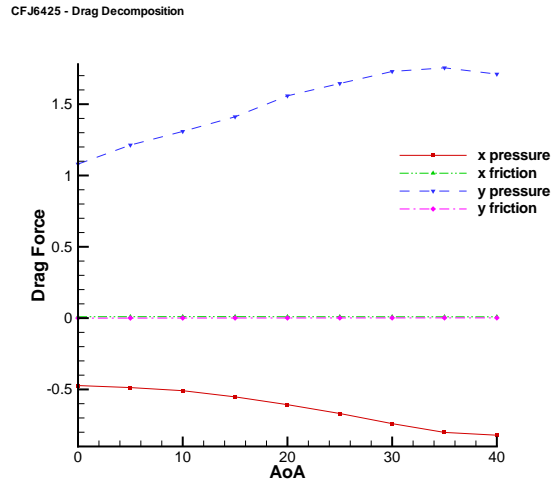


Figure 16: Drag breakdown at different angles of attack

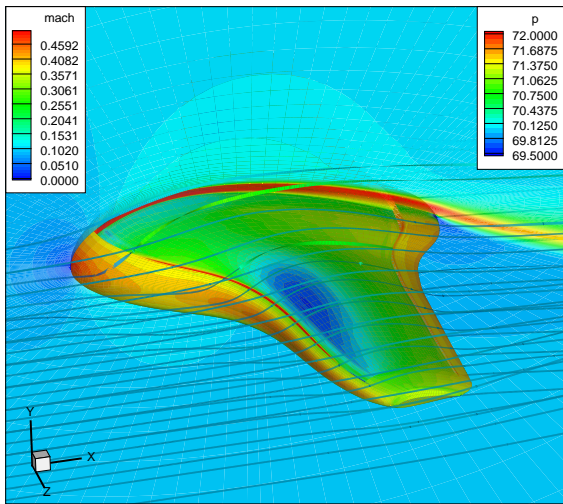


Figure 15: 3-D mach contours in midplane, pressure contours on surface, and 3D streamlines

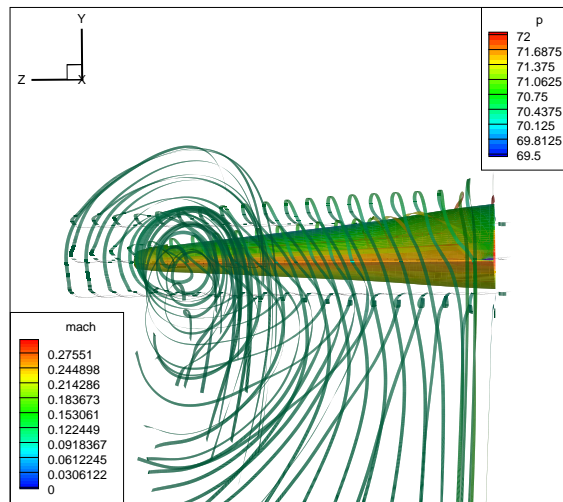


Figure 17: 3-D streamlines showing wing-tip vortices

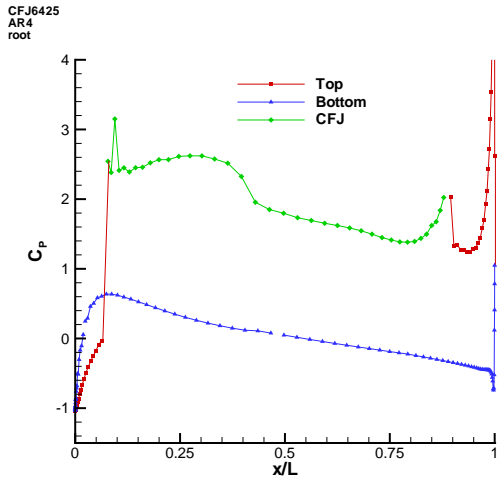


Figure 18: Distribution of pressure coefficient  $C_P$  over chord at wind root

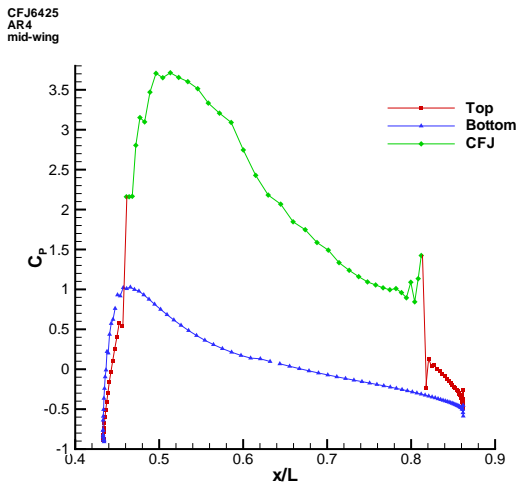


Figure 19: Distribution of pressure coefficient  $C_P$  over chord at mid-span